Patterning of $L1_0$ FePt nanoparticles with ultra-high coercivity for bit-patterned media

Zhengong Meng,‡a Guijun Li,‡b Hon-Fai Wong,b Sheung-Mei Ng,b Sze-Chun Yiu,a Cheuk-Lam Ho,*a Chi-Wah Leung,*b Ian Manners*c and Wai-Yeung Wong*ad

* Corresponding authors

a Institute of Molecular Functional Materials, Department of Chemistry and Institute of Advanced Materials, Hong Kong Baptist University, Waterloo Road, Kowloon Tong, Hong Kong, P. R. China

E-mail: rwywong@hkbu.edu.hk, clamho@hkbu.edu.hk

Fax: +852-3411-7348

b Department of Applied Physics, The Hong Kong Polytechnic University, Hung Hom, Hong Kong, P. R. China

E-mail: dennis.leung@polyu.edu.hk

c School of Chemistry, University of Bristol, Bristol, UK

E-mail: Ian.Manners@bristol.ac.uk

d Department of Applied Biology and Chemical Technology, The Hong Kong Polytechnic University, Hung Hom, Hong Kong, P. R. China

E-mail: wai-yeung.wong@polyu.edu.hk

Abstract

$L1_0$-ordered FePt nanoparticles (NPs) with ultra-high coercivity were directly prepared from a new metallopolyyne using a one-step pyrolysis method. The chemical ordering, morphology and magnetic properties of the as-synthesized FePt NPs have been studied. Magnetic measurements show the coercivity of these FePt NPs is as high as 3.6 T. Comparison of NPs synthesized under the Ar and Ar/H_2 atmospheres shows that the presence of H_2 in the annealing environment influences the nucleation and promotes the growth of $L1_0$-FePt NPs. Application of this metallopolymer for bit-patterned media was also demonstrated using nanoimprint lithography.

Introduction

The volume of hard disk drives (HDDs) has increased exponentially from 5 megabits (Mb) in the first IBM 350 disk storage unit to multiple terabits (Tb) in the disk drives currently available on the market. The storage capacities of conventional perpendicular magnetic recording systems are unlikely to be increased further because it is not easy to maintain a high signal-to-noise ratio (SNR) below 10 nm per bit due to the thermal instability of magnetic metal alloy materials.[1] Thus, it is important to develop new data recording architectures for increasing the areal density as well as the data stability in HDDs. A bit-patterned media (BPM) system, in which a single magnetic bit is recorded on a pre-defined single magnetic dot, has a higher SNR due to the absence of transition noise and erase bands, and it has emerged as a promising technology for extending magnetic data storage density beyond 1 Tb in^{-2}.[2] As reported by the Advanced Storage Technology Consortium, novel storage architectures from combining BPM and Heat-Assisted Magnetic Recording (HAMR) will lead to 10 Tb in^{-2} in the areal density by 2025. Furthermore, as demonstrated by Hitachi Global Storage Technologies (HGST), BPM will be improved towards higher areal density by utilizing nanolithography to break magnetic media down into small regions or bit “islands” on a platter's surface.[3]

Recently, the main preparation methods of BPM include electron-beam lithography (EBL),[4] directed self-assembly of block copolymer,[5–8] self-aligned double patterning[9] and nanoimprint lithography (NIL),[8,10–13] *etc*. Among these, NIL allows the fabrication of large-area nanometer scale patterns rapidly as BPM possesses good features such as low production cost, high throughput and high resolution.[14–16] Generally, there are two main steps in NIL patterning: the pre-patterning of the substrate with pillar features and the deposition of the magnetic film on the features.[15,17–19] For making BPM with a continual magnetic thin film using NIL, the

photoresist must first be spin-coated and patterned using NIL. Then, either the magnetic thin film is etched away (a subtractive process) or the thin film is deposited and lifted off (an additive process).[20]

A range of nanomaterials have been studied for the magnetic recording layer such as FePt,[21] FePd,[22] CoPt,[23] CoPd[24] and CoCrPt,[25] *etc*. In particular, $L1_0$-type FePt nanoparticles (NPs) with face-centered tetragonal (fct) structures were considered as a promising candidate for the next generation of ultrahigh-density data storage systems due to their large uniaxial magnetocrystalline anisotropy ($K_u \approx 7 \times 10^6$ J m^{-3}) and good chemical stability.[26–28] The previous approach of synthesizing FePt NPs often relied on vacuum-deposition techniques, however, multi-step procedures were generally required to prepare regular bit patterns.[29] Meanwhile, solution phase chemical synthesis was successfully adopted to prepare monodisperse FePt NPs since the first report by Sun *et al.* in 2000.[30] Patterned arrays of FePt NPs have also been fabricated using colloidal self-assembly based on the combination of physical patterning tools with self-assembly, but the mass production of such arrays is still a challenge as ordering of NPs is typically only over micrometer scale regions. Besides, although this method demonstrates the feasibility to produce nanocrystals with smooth morphologies, the dual-source precursors involved such as $Fe(CO)_5$ or $Fe(acac)_2$ and $Pt(acac)_2$, also bring about the difficulty for stoichiometric control.[30–32] Recently, single-source organometallic precursors such as $(CO)_3Fe(\mu\text{-dppm})(\mu\text{-CO})PtCl_2$ and $FePt(CO)_4dppmBr_2$ were reported,[33–37] in which the atomic ratio of Fe and Pt could be easily controlled. In such cases, the precursors would decompose at the same decomposition temperature and the two types of metal atoms were homogeneously distributed in the organic framework at the molecular scale, which would be beneficial to prevent the agglomeration of FePt NPs.

Metallopolymers are of intense interest owing to their ability to be easily processed and fabricated into films.[38–40] We have previously reported a series of Fe,Pt-containing metallopolymers as precursors to prepare $L1_0$-FePt NPs *via* one-pot pyrolysis under an inert atmosphere.[10,41,42] These single-source polymer precursors could also be used as photoresists to afford micro- or nano-patterns by EBL or NIL.[43,44] However, the coercivities of the as-synthesized FePt NPs are still relatively low, which would restrict their potential as magnetic data recording media. With the effort of searching for new approaches of preparing highly ordered FePt NPs, a new strategy for optimizing the synthetic process is reported in the present study. Here, a new bimetallic metallopolyyne polymer **P** of Fe and Pt was designed and synthesized, in which a ferrocene was symmetrically bonded to the aromatic ring through a freely-rotating O-bridge. This molecular design not only improves the overall solubility of the resulting polymer in common organic solvents, but also increases the solution processability of the polymer for the fabrication of nanoscale patterns *via* NIL.

Results and discussion

Synthesis and characterization of $L1_0$-FePt nanoparticles

The synthesis of metallopolymer **P** was carried out using a Cu(I)-catalyzed dehydrohalogenation reaction between $PtCl_2$(4,4′-dinonyl-2,2′-bipyridyl) and diethynyl ligand **3** (Scheme 1). Ferrocene, used as the Fe source in **P**, was bonded to the phenyl ring by a freely-rotating O-bridge, which could improve the solubility of the resulting polymer in common organic solvents. In addition, the diethynyl ligand, **3**, has a symmetrical structure and, therefore, the two terminal acetylenic protons show similar reactivity, which can facilitate the final polymer having a higher molecular weight and further enhance the interactions among different polymer molecules.

The polymer **P**, used as the single-source precursor for the FePt NPs, was put in a ceramic boat, which was placed in a tube furnace. The tube was purged for 30 min, and then heated to 800 °C and kept for 1 h under an Ar/H_2 (v/v = 95/5) atmosphere. The resulting black powder, containing FePt NPs, was removed from the furnace after cooling the tube slowly to room temperature. The as-synthesized FePt NPs were then characterized using wide-angle X-ray diffraction (XRD) and transmission electron microscopy (TEM) to investigate their phase and morphology.

The representative TEM micrographs of the as-synthesized FePt NPs at low and high resolution are shown in Fig. 1a and b. The NPs had regular shapes with good contrast at low magnification, and were evenly dispersed on the amorphous carbon matrix, which could immobilize and protect the FePt alloys. The sizes of the resultant NPs were statistically analyzed from a wide area, as shown in Fig. 1c. The mean size was about 12.7 nm with a standard deviation of 1.4 nm, which was in good agreement with the calculated results determined by the (111) diffraction peak position in the powder XRD (PXRD) spectrum. The measured lattice fringes of 0.221 and 0.283 nm from the high resolution TEM image (Fig. 1b) of the individual single-crystal NPs are consistent with the *d*-spacing known for the (111) and (110) planes of fct FePt NPs, which reveals that the resultant FePt NPs possess a highly ordered fct structure.

Fig. 1d shows the PXRD patterns of the resultant FePt NPs. Well-resolved diffraction peaks were observed and indexed to the typical peaks of FePt (JCPDS card no. 043-1359) alloys. The appearance of the strong (001) and (110) peaks in the curve suggests that the NPs have a chemically ordered fct structure, and the obvious splitting of the (200)/(002) and (220)/(202) pairs of reflections indicates that the $L1_0$ phase has a very high degree of ordering. The mean

crystallite size was estimated to be 12.9 nm from the full width at the half-maximum of the (111) peak by the Scherrer analysis.

The composition of the resulting nanomaterials was studied using energy-dispersive X-ray (EDX) elemental analysis. The EDX result (see ESI, Fig. S1†) shows that the ratio of Fe to Pt in NPs was around 0.45 : 0.55, which is within the experimental error for the ratio determined by the (111) diffraction peak position in the PXRD spectrum.

The magnetic hysteresis loop was measured at room temperature on a physical property measurement system (PPMS) and the result is shown in Fig. 2. The saturation moment (M_s) was obtained when an external field up to 9 T (1 T = 10 kOe) was applied. The magnetic properties of the as-synthesized FePt NPs revealed ferromagnetic features. In addition, it was found that the NPs had a room-temperature coercivity H_c of 3.6 T and a saturated moment M_s of 19.8 emu g^{-1}. Such a large coercivity further verified that the NPs indeed possessed a highly ordered $L1_0$ structure. As compared to the FePt NPs prepared from similar methods reported in the literature, the coercivity in the present study was significantly increased from 1.4 T to 3.6 T,[10,41,42] which is even larger than the value (3.3 T) reported by Sun *et al.*[45] To our knowledge, this value represents the largest magnetic coercivity value for $L1_0$-FePt NPs ever reported. We believe that the main difference lies in the fact that the fct FePt NPs herein were synthesized under an Ar/H_2 atmosphere, where H_2 could be adsorbed on the surface of the seeds of NPs during nucleation to hinder seed aggregation and further promote growth on the seed surface.[46] Furthermore, since the Fe and Pt sources were alternately linked with the organic linkages, this would promote the formation of fct FePt NPs as the $L1_0$-FePt phase can be considered as a superlattice of Fe and Pt atoms stacked along the [001] direction.

To verify this hypothesis, FePt NPs were also synthesized according to the previously reported pyrolysis conditions: **P** was pyrolyzed for 1 h under an Ar atmosphere to prepare the FePt NPs. The resultant NPs had a smaller size of *ca*. 5.3 nm with a standard deviation of 1.2 nm as statistically analyzed from the TEM image (Fig. S2†), and the atomic ratio 46 : 54 of Fe to Pt was verified by the EDX spectrum (Fig. S3†). PXRD was also applied to identify the phase and crystallinity of the NPs (Fig. S4†). The (001) and (110) characterization peaks of fct-phase FePt NPs were observed, but the intensity was relatively weak for the (001) plane. In addition, the splitting of the (200) and (220) peaks was also not clearly observed. It could be deduced that the resultant FePt NPs were not highly ordered, or existed as a mixture of the fcc and fct phases. The magnetic hysteresis loop (Fig. S5†) was also measured and the resulting lower coercivity of 0.75 T further supported this conclusion. All of these results indicate the merit of introducing H_2 in promoting the synthesis of $L1_0$-FePt NPs.

Patterning of $L1_0$-FePt nanoparticles using nanoimprint lithography

The improvement of material properties to push data storage density beyond the Tb in^{-2} value is important for high-density data storage applications. Therefore, patterning of the $L1_0$-FePt alloy NPs with a high degree of order and high K_u is an effective strategy to achieve the goal. In our previous reports, the polymer precursors were successfully patterned on the Si substrate using EBL and NIL, respectively.[10,42] Particularly, NIL was considered as a high throughput process to fabricate various patterns at the nanometer scale. In the present study, the new metallopolymer **P** acts as a photoresist, and a saturated solution in chloroform was first drop-cast onto the Si substrate. Then the poly(dimethylsiloxane) (PDMS) templates were cast onto the substrate; the stamps used in this study included a line array in one dimension with a periodicity

of 740 nm (feature size of 350 nm) and a dot array in two dimensions with a periodicity of 500 nm (feature size of 250 nm). After the solvent was evaporated, the templates were lifted off and the reverse patterns of **P** were left on the substrate. Finally, the highly ordered 2D ferromagnetic arrays were obtained by annealing the pre-pattern under an Ar/H_2 atmosphere.

As displayed in Fig. 3, regular line arrays were fabricated. The SEM images in Fig. 3a and b show the line patterns of **P** and the ferromagnetic FePt NPs obtained after pyrolysis, respectively. As depicted from Fig. 3a, the pattern and structure of the imprinted bimetallic FePt-containing polymer **P** can be controlled and defined by the stamp. Also, the morphology of the line arrays revealed the same feature size before and after pyrolysis (Fig. 3a and b). However, because the polymer skeleton was collapsed during pyrolysis, the height of the ferromagnetic line was decreased dramatically from 100 nm to 30 nm after pyrolysis. Fig. 3c and d illustrate the top view 2D and 3D AFM images corresponding to Fig. 3b, respectively, which further proved that the line arrays still preserve their highly ordered patterns after pyrolysis.

In order to isolate each magnetic recording bit within the bit-patterned media architecture, the PDMS template with hole array stamps was used to fabricate the negative patterns with dot arrays. Fig. 4a portrays the SEM image of nanoimprinted polymer **P** with a nanodot array pattern, in which the periodicity of 500 nm and feature size of 250 nm were observed. The patterned substrate was then annealed for 1 h at 800 °C under an Ar/H_2 atmosphere; the polymer precursor was decomposed to form $L1_0$-FePt NPs through epitaxial growth. As demonstrated in the AFM images in Fig. 4b, the morphology of the dot pattern was preserved after pyrolysis, and the 3D AFM image in Fig. 4d intuitively shows the regular patterns of the dot array structure on the substrate. The height of the dot array was measured to be around 10 nm, which was shown clearly by the cross-section profile in Fig. 4c. This was relatively small compared to the depth of

the original PDMS mold (80 nm) owing to the collapse of the polymer skeleton during pyrolysis. In addition, the magnetic properties were characterized by magnetic force microscopy (MFM). Fig. 4e shows the corresponding MFM image. A nanopattern of magnetization with the same periodicity as the dot array pattern in the corresponding AFM image (Fig. 4b) can be observed clearly, which indicates that this dot array nanopattern is magnetic and thereby can be used as a new platform for future perpendicular ultrahigh-density magnetic data recording. Our prototype BPM provides here an areal density of 2.58 Gb in^{-2}. In addition, the higher coercivity means more stable bits, which gives FePt NPs good potential to be developed as stable BPMs with higher areal density.

Experimental

General procedure and materials

All reactions were carried out under nitrogen unless otherwise stated. Commercially available reagents were used as received without further purification. 1,3-Dibromo-2-(bromomethyl)benzene and $PtCl_2$(4,4′-dinonyl-2,2′-bipyridyl) were prepared *via* the literature methods.[10] Other reagents were purchased and used as received. All reactions were monitored using thin-layer chromatography (TLC) with Merck pre-coated glass plates. Compounds were visualized with UV light irradiation at 254 and 365 nm. Separation or purification of products was achieved using column chromatography. NMR spectra were measured in $CDCl_3$ on a Bruker AV 400 NMR instrument with chemical shifts referenced against tetramethylsilane as the internal standard for ^{1}H, and ^{13}C NMR data. The molecular weight of the polymer was determined using gel permeation chromatography (GPC) using a HP 1050 series HPLC instrument with visible wavelength and fluorescent detectors against polystyrene standards.

Synthesis of FePt-containing polymer P

Ferrocenylmethanol: Ferrocenecarboxaldehyde (0.54 g, 2.5 mmol) and $NaBH_4$ (0.12 g, 3 mmol) were dissolved in EtOH (30 mL), and H_2O (1 mL) was then added dropwise to the solution. The mixture was stirred for 1 h and then refluxed for another 2 h. After cooling to room temperature, the solvent was removed and the crude product was extracted with Et_2O (3 × 50 mL). The organic phase was dried and the residue was recrystallized in *n*-hexane to get the pure product as a yellow solid (0.49 g, 90%). ^{1}H NMR (400 MHz, $CDCl_3$, δ): 4.24 (t, J = 2 Hz, 2H, Fc–H), 4.20 (t, J = 0.8 Hz, 2H, Fc–H), 4.17 (s, 5H, Fc–H), 1.66 (s, 2H, –CH_2–), 1.60 (broad, 1H, –OH); ^{13}C NMR (100 MHz, $CDCl_3$, δ): 88.5, 68.4, 68.3, 68.0 (Fc), 60.8 (–CH_2–).

1: To a solution of ferrocenylmethanol (0.43 g, 2.0 mmol) in dry THF (10 mL), NaH (0.12 g, 3 mmol) was added slowly at 0 °C under a nitrogen atmosphere. After stirring for 0.5 h, 1,3-dibromo-5-(bromomethyl)benzene (0.66 g, 2.0 mmol) in THF (10 mL) was added dropwise and the reaction mixture was stirred overnight at 60 °C. The reaction mixture was quenched with saturated aq. NH_4Cl (50 mL) at 0 °C and extracted with CH_2Cl_2 (3 × 50 mL). The combined organic extracts were washed with brine, dried over anhydrous Na_2SO_4 and concentrated under reduced pressure. The residue was purified using column chromatography on silica gel using *n*-hexane/dichloromethane (1 : 3, v/v) as the eluent to afford a yellow solid (0.69 g, 74%). ^{1}H NMR (400 MHz, $CDCl_3$, δ): 7.57 (s, 1H, Ar–H), 7.41 (s, 2H, Ar–H), 4.43 (s, 2H, –CH_2–), 4.34 (s, 2 H, –CH_2–), 4.24 (t, J = 2 Hz, 2H, Fc–H), 4.18 (t, J = 1.6 Hz, 2H, Fc–H), 4.14 (s, 5H, Fc–H); ^{13}C NMR (100 MHz, $CDCl_3$, δ): 142.7, 133.0, 129.1, 122.9 (Ar), 82.8, 70.0, 69.5, 68.9 (Fc), 68.7, 68.5 (–CH_2–).

2: To an ice-cooled mixture of **3** (2.05 g, 6.6 mmol) in freshly distilled triethylamine (25 mL) and dichloromethane (25 mL) solution was added $Pd(PPh_3)_4$ (200 mg) and CuI (50 mg). After

the solution was stirred for 30 min at 0 °C, trimethylsilylacetylene (5 mL) was then added and the suspension was stirred for 30 min in an ice-bath before being warmed to room temperature. After reacting for 30 min at room temperature, the mixture was heated to 75 °C for 24 h. The solution was then allowed to cool to room temperature and the solvent mixture was evaporated *in vacuo*. The crude product was purified using column chromatography on silica gel using *n*-hexane/dichloromethane (1 : 3, v/v) as the eluent to provide compound **2** as an orange solid (1.78 g, 81%). IR (KBr): 2126 cm^{-1} (C≡C); ^{1}H NMR (400 MHz, $CDCl_3$, δ): 7.50 (s, 1H, Ar–H), 7.38 (s, 2H, Ar–H), 4.43 (s, 2H, $–CH_2–$), 4.31 (s, 2 H, $–CH_2–$), 4.24 (t, J = 2 Hz, 2H, Fc–H), 4.17 (t, J = 2 Hz, 2H, Fc–H), 4.13 (s, 5H, Fc–H), 0.24 (s, 9H, –TMS); ^{13}C NMR (100 MHz, $CDCl_3$, δ): 139.1, 134.5, 130.9, 123.5 (Ar), 104.1, 95.0 (C≡C), 83.1, 70.6, 69.5, 68.7 (Fc), 68.6, 68.5 ($–CH_2–$), 0.0 (–TMS).

3: Compound **2** (0.99 g, 2 mmol) and excess K_2CO_3 (0.41 g, 3 mmol) were dissolved in MeOH/CH_2Cl_2 (30 mL, v/v = 1/1) and the mixture was stirred overnight at room temperature. It was then washed with water and extracted with CH_2Cl_2. The organic phase was combined and evaporated under vacuum. The crude product was purified using column chromatography on silica gel using *n*-hexane/dichloromethane (1 : 4, v/v) as the eluent to provide **3** in a quantitative yield. IR (KBr): 2105 cm^{-1} (C≡C), 3320 cm^{-1} (C≡C–H); ^{1}H NMR (400 MHz, $CDCl_3$, δ): 7.52 (s, 1H, Ar–H), 7.44 (s, 2H, Ar–H), 4.45 (s, 2H, $–CH_2–$), 4.33 (s, 2 H, $–CH_2–$), 4.24 (t, J = 1.6 Hz, 2H, Fc–H), 4.17 (t, J = 2 Hz, 2H, Fc–H), 4.13 (s, 5H, Fc–H), 3.08 (s, 2H, –C≡CH); ^{13}C NMR (100 MHz, $CDCl_3$, δ): 139.4, 134.7, 131.4, 122.6 (Ar), 83.0, 82.6 (C≡C), 78.0, 70.5, 69.5, 68.7 (Fc), 68.6, 68.5 ($–CH_2–$).

P: A mixture of **3** (70.8 mg, 0.02 mmol), $PtCl_2$(4,4′-dinonyl-2,2′-bipyridyl) (134.9 mg, 0.02 mmol) and CuI (1 mg) in $CHCl_3$/i-Pr_2NH (30 mL, v/v = 1/1) was stirred for 24 h at 40 °C. The

solvent was removed under vacuum and then the residue was redissolved in CH_2Cl_2 and filtered through a short alumina column to give a solution of **P**. After removal of the solvents, the solid was dissolved in a small amount of CH_2Cl_2 and precipitated from methanol. IR (KBr): 2105 cm^{-1} (C≡C); ^1H NMR (400 MHz, $CDCl_3$, δ): 9.52–9.36 (m, 2H, Ar–H), 8.93–8.74 (m, 2H, Ar–H), 8.56–8.15 (m, 2H, Ar–H), 7.94–7.61 (m, 3H, Ar–H), 4.74 (s, 2H, Ar–H), 4.74–4.08 (m, 13H, Fc–H and Ar–CH_2–), 3.41 (s, 2H, C≡CH), 2.72 (s, 4H, –CH_2–), 1.65 (s, 4H, –CH_2–), 1.22–1.12 (m, 24H, –CH_2–), 0.83 (s, 6H, CH_3). GPC (THF): M_w = 8690, M_n = 5020, PDI = M_w/M_n = 1.73. TGA (heating rate 10 °C min^{-1}): T_{onset}: 264 ± 5 °C.

Preparation of FePt nanoparticles

In metallopolymer **P**, the Fe and Pt sources are evenly dispersed in the same molecule and bonded chemically, which means that **P** can act as a single-source precursor to prepare FePt NPs. Polymer **P** was put in a ceramic boat and was then placed in a tube furnace equipped with temperature and gas-flow controls. The precursor was heated for 1 h under an Ar/H_2 atmosphere at 800 °C. After being cooled to room temperature, black powdery FePt NPs were formed. The resultant nanomaterials were then characterized using PXRD, TEM, EDX and PPMS.

Patterning of FePt nanoparticles

A solution of **P** in chloroform (20 mg mL^{-1}) was prepared and filtered using a syringe with a 0.22 μm pore size hydrophobic Nylon membrane. 20 μL of the solution was drop-cast onto a Si wafer (10 × 10 mm^2), which had previously been cleaned with acetone. Then a PDMS template with stamps, such as a line or dot array, was immediately imprinted onto the wafer for 5 min under 1 N cm^{-2} of pressure. After removing the template, the reverse stamps of the

polymer **P** were left on the Si substrate. The substrate was annealed to get the ferromagnetic patterns according to the same pyrolysis conditions as for the preparation of FePt NPs.

Conclusions

$L1_0$-FePt NPs with highly ordered crystalline structures were prepared from the single-source bimetallic metallopolymer precursor **P**. Pyrolysis of **P** under an Ar/H_2 atmosphere successfully produced the resultant FePt NPs with an ultra-high coercivity of 3.6 T, where the existence of H_2 played an important role in facilitating the formation of the fct phase. The metallopolymer precursor was easily used as a photoresist and could be directly imprinted on the desired substrate. Ferromagnetic 2D line and dot arrays suitable for BPM were patterned, which are potentially useful for high-density data storage applications. In principle, the approach can be readily extended to other $L1_0$-phase nanocrystals (NC) such as CoPt and FePd. Therefore, the present work opens up a new and general route for the fabrication of highly ordered 2D ferromagnetic NP arrays.

Acknowledgements

W.-Y. Wong thanks the Hong Kong Research Grants Council (HKBU 12302114), Areas of Excellence Scheme of HKSAR (AoE/P-03/08), National Natural Science Foundation of China (Project No. 51373145), Science, Technology, and Innovation Committee of Shenzhen Municipality (JCYJ20140419130507116), Hong Kong Baptist University (FRG2/13-14/083) and the Hong Kong Polytechnic University for financial support. C.-L. Ho thanks Hong Kong Baptist University (FRG2/13-14/078), and the Science, Technology and Innovation Committee of Shenzhen Municipality (JCYJ20140818163041143) for their financial support. We also thank

the National Natural Science Foundation of China (project number: 21504074). The work in PolyU was supported by the Hong Kong Research Grants Council (PolyU 153015/14P) and PolyU (1-ZE14/1-ZE25).

Graphical image

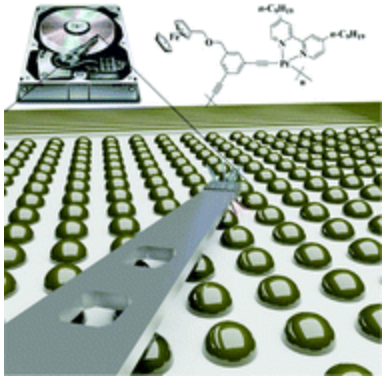

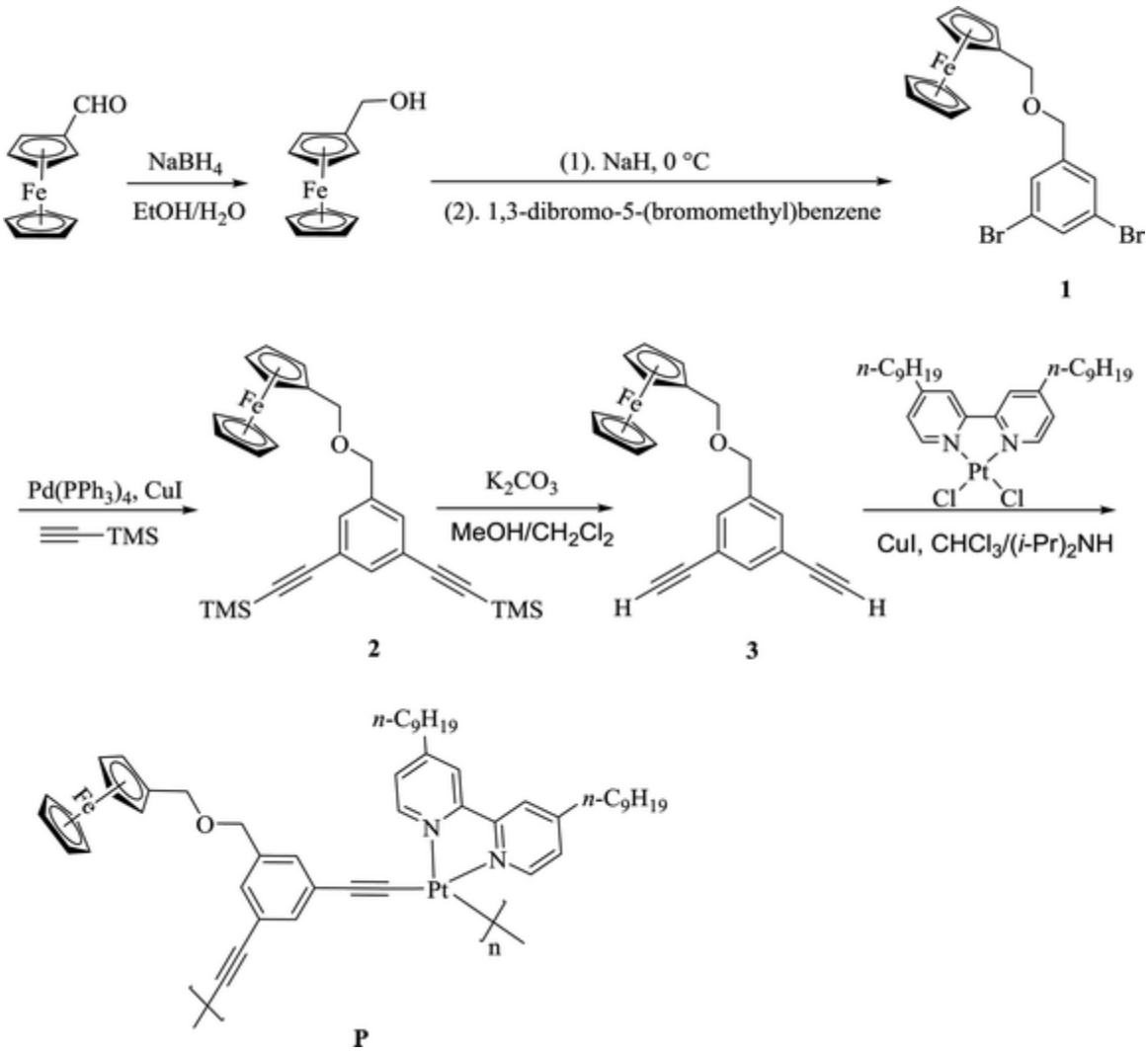

Scheme 1 Synthetic route to FePt-containing polymer **P**.

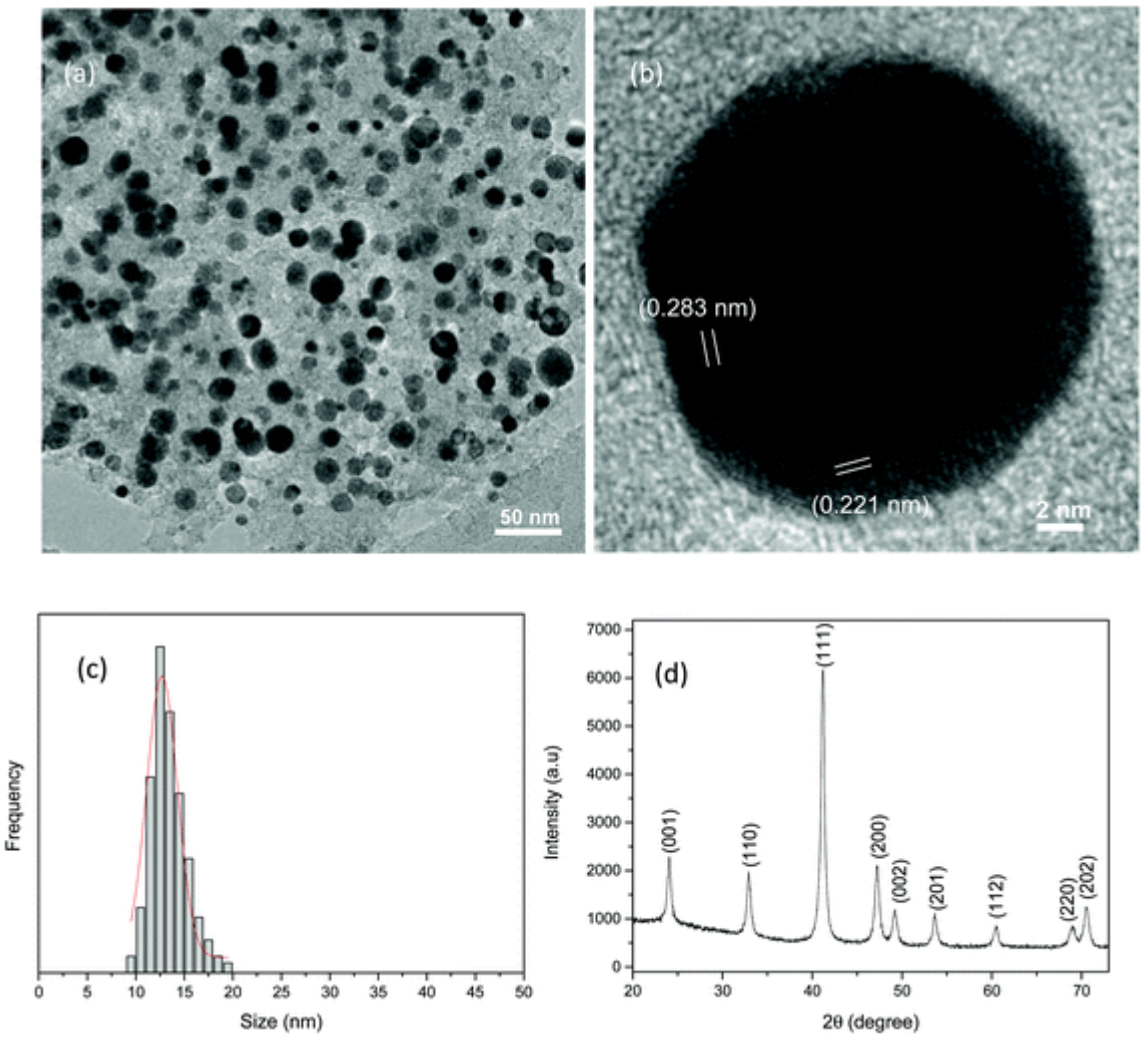

Fig. 1 (a) Low-resolution TEM image of the resultant FePt NPs; (b) high-resolution TEM image with lattice fringes; (c) size distribution of FePt NPs determined by statistical analysis from the TEM images and (d) XRD pattern of FePt NPs synthesized from the precursor **P**.

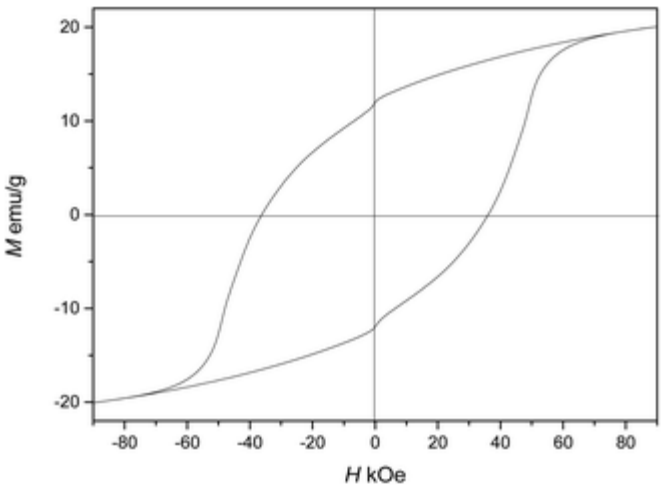

Fig. 2 Magnetic hysteresis loop of the fct-FePt NPs measured at room temperature.

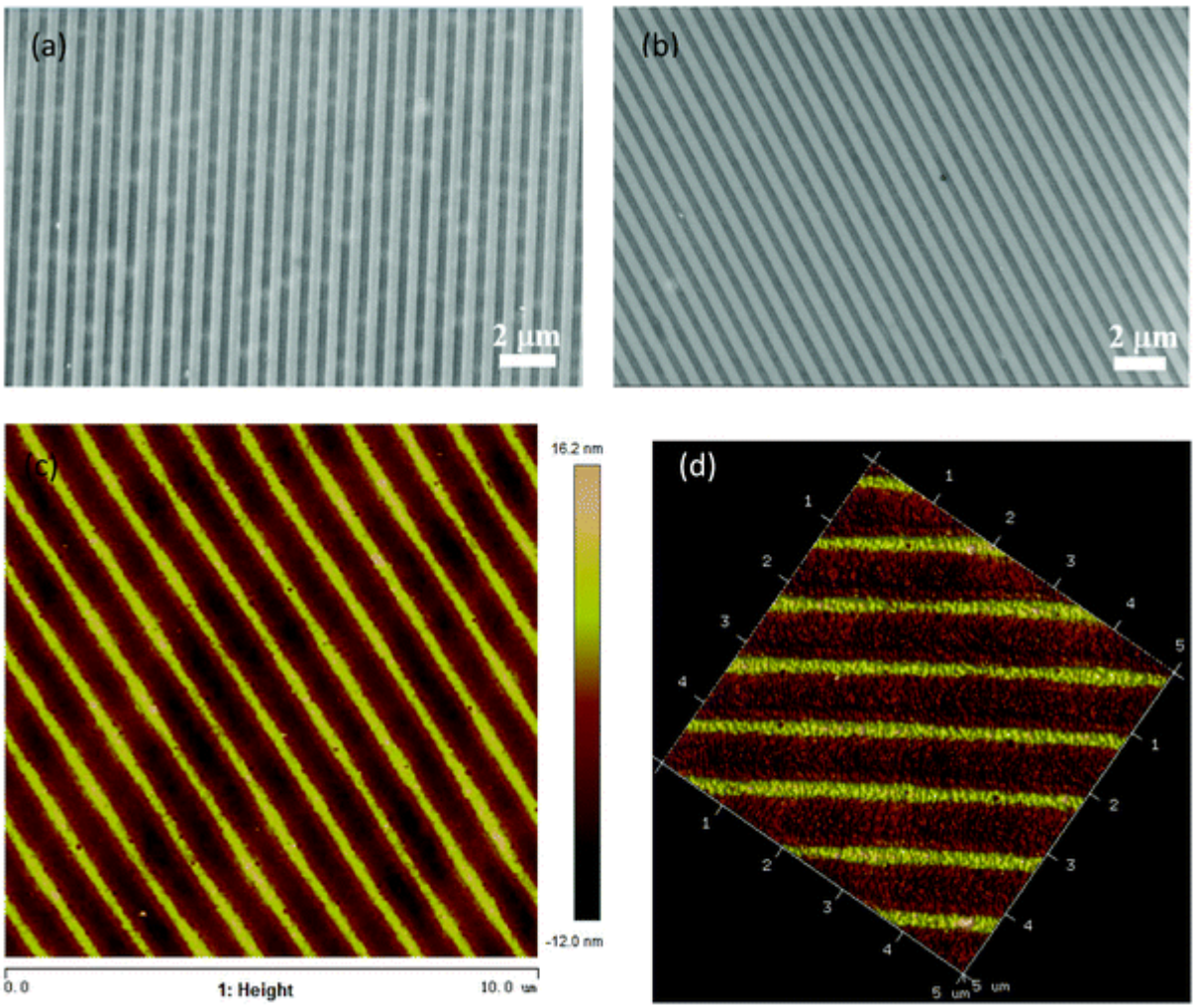

Fig. 3 (a) SEM image of the regular line arrays of polymer **P** patterned on the Si substrate; (b–d) SEM, 2-D and 3-D AFM images of the as-synthesized ferromagnetic line pattern of FePt NPs after pyrolysis under an Ar/H_2 atmosphere (v/v = 95/5). 3D AFM image size 5 × 5 μm^2.

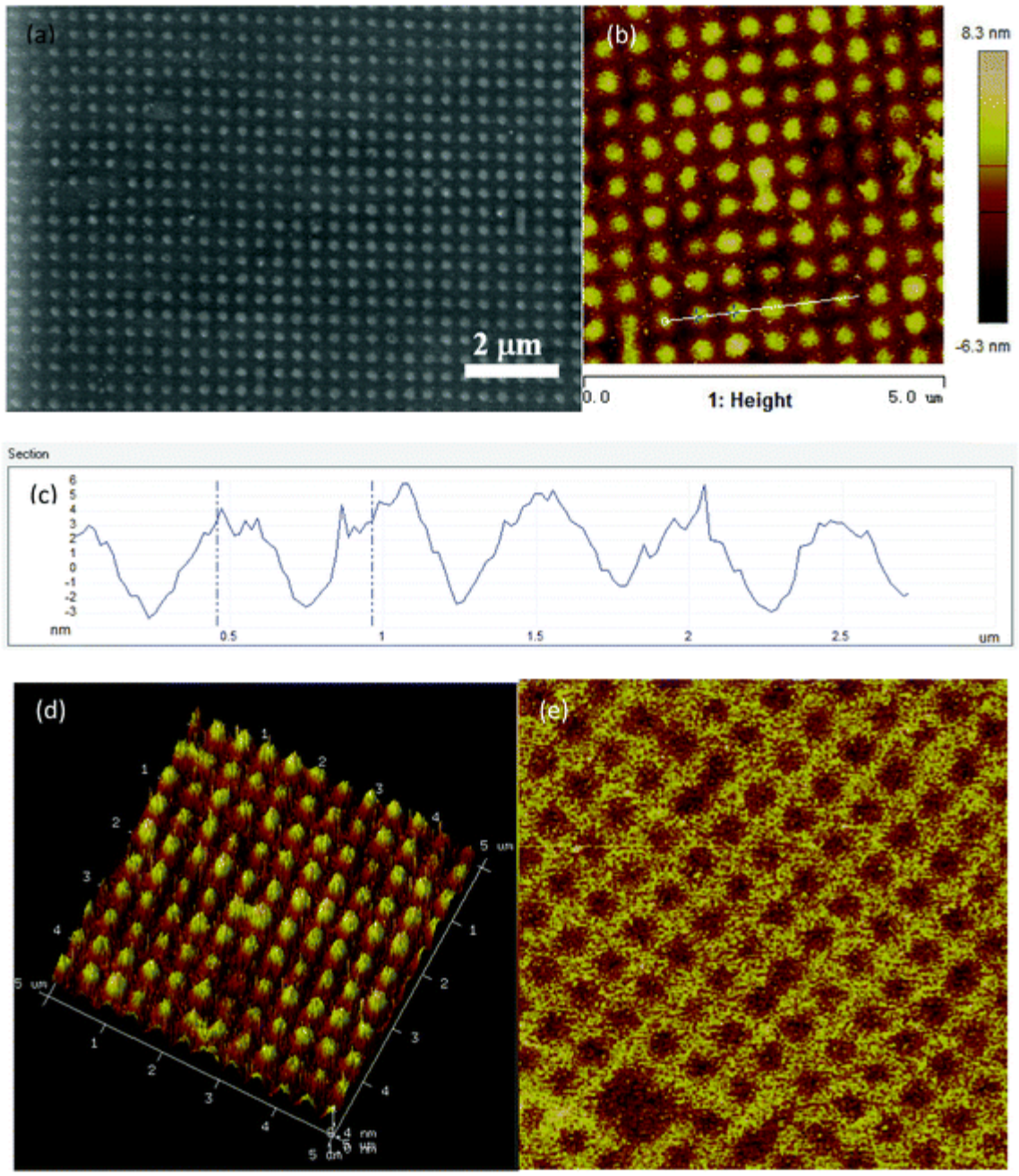

Fig. 4 (a) SEM image of regular dot arrays of **P** patterned on the Si substrate; (b) 2D AFM image of the as-synthesized ferromagnetic line pattern of FePt NPs after pyrolysis under Ar/H_2 (v/v = 95/5); (c) cross-section of (b); (d) 3D AFM image of (b); (e) MFM image of (b). AFM and MFM image sizes: 5×5 µm^2.

Notes and references

1 D. A. Thompson and J. S. Best, IBM J. Res. Dev., 2000, 44, 311.

2 T. R. Albrecht, H. Arora, V. Ayanoor-Vitikkate, J. M. Beaujour, D. Bedau, D. Berman, A. L. Bogdanov, Y. A. Chapuis, J. Cushen, E. E. Dobisz, G. Doerk, H. Gao, M. Grobis, B. Gurney, W. Hanson, O. Hellwig, T. Hirano, P. O. Jubert, D. Kercher, J. Lille, Z. W. Liu, C. M. Mate, Y. Obukhov, K. C. Patel, K. Rubin, R. Ruiz, M. Schabes, L. Wan, D. Weller, T. W. Wu and E. Yang, IEEE Trans. Magn., 2015, 51, 0800342.

3 Lucas Mearian, Couputerworld. Want a 100TB disk drive? You'll have to wait 'til 2025. See: http://www.computerworld.com/article/2852233/want-a-100tb-disk-drive-youllhave-to-wait-til-2025.html, accessed: Nov, 2014.

4 M. T. Moneck, T. Okada, J. Fujimori, T. Kasuya, M. Katsumura, T. Iida, K. Kuriyama, W. C. Lin, V. Sokalski, S. P. Powell, J. A. Bain and J. G. Zhu, IEEE Trans. Magn., 2011, 47, 2656.

5 X. M. Yang, S. G. Xiao, Y. Hsu, M. Feldbaum, K. Lee and D. Kuo, J. Nanomater., 2013, 615896.

6 R. Ruiz, E. Dobisz and T. R. Albrecht, ACS Nano, 2011, 5, 79.

7 J. K. Bosworth, E. Dobisz and R. Ruiz, J. Photopolym. Sci. Technol., 2010, 23, 145.

8 X. M. Yang, L. Wan, S. G. Xiao, Y. A. Xu and D. K. Weller, ACS Nano, 2009, 3, 1844.

9 C. Bencher, Y. Chen, H. Dai, W. Montgomery and L. Huli, Proc. SPIE, 2008, 6924, 69244E.

10 Q. Dong, G. J. Li, C.-L. Ho, M. Faisal, C. W. Leung, P. W. T. Pong, K. Liu, B. Z. Tang, I. Manners and W.-Y. Wong, Adv. Mater., 2012, 24, 1034.

11 X. M. Yang, Y. Xu, K. Lee, S. G. Xiao, D. Ku and D. Weller, IEEE Trans. Magn., 2009, 45, 833.

12 J. S. Sohn, D. Lee, E. Cho, H. S. Kim, B. K. Lee, M. B. Lee and S. J. Suh, Nanotechnology, 2009, 20, 025302. 13 Z. Li, W. Zhang and K. M. Krishnan, AIP Adv., 2015, 5, 087165.

14 B. D. Gates, Q. B. Xu, M. Stewart, D. Ryan, C. G. Willson and G. M. Whitesides, Chem. Rev., 2005, 105, 1171.

15 G. J. Li, C. W. Leung, Z. Q. Lei, K. W. Lin, P. T. Lai and P. W. T. Pong, Thin Solid Films, 2011, 519, 8307.

16 S. Y. Chou, P. R. Krauss and P. J. Renstrom, Science, 1996, 272, 85.

17 M. D. Austin and S. Y. Chou, Nano Lett., 2003, 3, 1687.

18 S. Y. Chou, P. R. Krauss, W. Zhang, L. J. Guo and L. Zhuang, J. Vac. Sci. Technol., B, 1997, 15, 2897.

19 S. Y. Chou, P. R. Krauss and P. J. Renstrom, Appl. Phys. Lett., 1995, 67, 3114.

20 P. A. Shields and D. W. E. Allsopp, Microelectron. Eng., 2011, 88, 3011.

21 A. T. McCallum, P. Krone, F. Springer, C. Brombacher, M. Albrecht, E. Dobisz, M. Grobis, D. Weller and O. Hellwig, Appl. Phys. Lett., 2011, 98, 242503.

22 L. Szunyogh, J. Zabloudil, A. Vernes, P. Weinberger, B. Ujfalussy and C. Sommers, Phys. Rev. B: Condens. Matter, 2001, 63, 184408.

23 V. W. Guo, H. S. Lee and J. G. Zhu, J. Appl. Phys., 2011, 109, 093908.

24 T. Hauet, O. Hellwig, S. H. Park, C. Beigne, E. Dobisz, B. D. Terris and D. Ravelosona, Appl. Phys. Lett., 2011, 98, 172506.

25 E. A. Dobisz, D. Kercher, M. Grobis, O. Hellwig, E. E. Marinero, D. Weller and T. R. Albrecht, J. Vac. Sci. Technol., B, 2012, 30, 06FH01.

26 D. Weller, A. Moser, L. Folks, M. E. Best, W. Lee, M. F. Toney, M. Schwickert, J. U. Thiele and M. F. Doerner, IEEE Trans. Magn., 2000, 36, 10.

27 S. H. Sun, Adv. Mater., 2006, 18, 393.

28 N. A. Frey, S. Peng, K. Cheng and S. H. Sun, Chem. Soc. Rev., 2009, 38, 2532.

29 S. Stappert, B. Rellinghaus, M. Acet and E. F. Wassermann, J. Cryst. Growth, 2003, 252, 440.

30 S. H. Sun, C. B. Murray, D. Weller, L. Folks and A. Moser, Science, 2000, 287, 1989.

31 M. Chen, J. P. Liu and S. H. Sun, J. Am. Chem. Soc., 2004, 126, 8394.

32 K. E. Elkins, T. S. Vedantam, J. P. Liu, H. Zeng, S. H. Sun, Y. Ding and Z. L. Wang, Nano Lett., 2003, 3, 1647.

33 A. Capobianchi, M. Colapietro, D. Fiorani, S. Foglia, P. Imperatori, S. Laureti and E. Palange, Chem. Mater., 2009, 21, 2007.

34 M. S. Wellons, W. H. Morris, Z. Gai, J. Shen, J. Bentley, J. E. Wittig and C. M. Lukehart, Chem. Mater., 2007, 19, 2483.

35 H. M. Song, J. H. Hong, Y. B. Lee, W. S. Kim, Y. Kim, S. J. Kim and N. H. Hur, Chem. Commun., 2006, 1292.

36 A. Siani, B. Captain, O. S. Alexeev, E. Stafyla, A. B. Hungria, P. A. Midgley, J. M. Thomas, R. D. Adams and M. D. Amiridis, Langmuir, 2006, 22, 5160.

37 R. D. Rutledge, W. H. Morris, M. S. Wellons, Z. Gai, J. Shen, J. Bentley, J. E. Wittig and C.M. Lukehart, J. Am. Chem. Soc., 2006, 128, 14210.

38 P. Nguyen, P. Gómez-Elipe and I. Manners, Chem. Rev., 1999, 99, 1515.

39 J. C. Eloi, L. Chabanne, G. R. Whittell and I. Manners, Mater. Today, 2008, 11, 28.

40 G. R. Whittell, M. D. Hager, U. S. Schubert and I. Manners, Nat. Mater., 2011, 10, 176.

41 Q. C. Dong, G. J. Li, H. Wang, P. W. T. Pong, C. W. Leung, I. Manners, C.-L. Ho, H. Li and W.-Y. Wong, J. Mater. Chem. C, 2015, 3, 734.

42 K. Liu, C.-L. Ho, S. Aouba, Y. Q. Zhao, Z. H. Lu, S. Petrov, N. Coombs, P. Dube, H. E. Ruda, W.-Y. Wong and I. Manners, Angew. Chem., Int. Ed., 2008, 47, 1255.

43 G. J. Li, Q. C. Dong, J. Z. Xin, C. W. Leung, P. T. Lai, W.-Y. Wong and P. W. T. Pong, Microelectron. Eng., 2013, 110, 192.

44 Z. G. Meng, G. J. Li, S. M. Ng, H. F. Wong, S. C. Yiu, C. L. Ho, C. W. Leung and W. Y. Wong, Polym. Chem., 2016, 7, 4467.

45 Q. Li, L. H. Wu, G. Wu, D. Su, H. F. Lv, S. Zhang, W. L. Zhu, A. Casimir, H. Y. Zhu, A. Mendoza-Garcia and S. H. Sun, Nano Lett., 2015, 15, 2468.

46 B. R. Bian, W. X. Xia, J. Du, J. Zhang, J. P. Liu, Z. H. Guo and A. R. Yan, IEEE Trans. Magn., 2013, 49, 3307.